Anomalous compressibility of ferropericlase throughout the iron spin cross-over

R. M. Wentzcovitch[a,b,1], J. F. Justo[a,b,c], Z. Wu[a,b], C. R. S. da Silva[b], D. A. Yuen[b,d], and D. Kohlstedt[d]

[a]Department of Chemical Engineering and Materials Science, [b]Minnesota Supercomputing Institute; and [d]Department of Geology and Geophysics, University of Minnesota, Minneapolis, MN 55455; and [c]Escola Politécnica, Universidade de São Paulo, CP 61548, CEP 05424-970, São Paulo, Brazil

The thermoelastic properties of ferropericlase $Mg_{1-x}Fe_xO$ (x = 0.1875) throughout the iron high-to-low spin cross-over have been investigated by first principles at Earth's lower mantle conditions. This cross-over has important consequences for elasticity such as an anomalous bulk modulus (K_S) reduction. At room temperature the anomaly is somewhat sharp in pressure but broadens with increasing temperature. Along a typical geotherm it occurs across most of the lower mantle with a more significant K_S reduction at ≈1,400–1,600 km depth. This anomaly might also cause a reduction in the effective activation energy for diffusion creep and lead to a viscosity minimum in the mid-lower mantle, in apparent agreement with results from inversion of data related with mantle convection and postglacial rebound.

Earth's lower mantle | viscosity | thermodynamics | thermal expansivity

Understanding of the Earth's lower mantle relies on indirect lines of evidence. Comparison of elastic properties extracted from seismic models with computed or measured elastic properties of candidate minerals at mantle conditions is a fruitful line of enquiry. For instance, it has shed light on the lower mantle composition (1–3) and on the nature of the D″ layer (4, 5). Such comparisons support the notion that the lower mantle consists primarily of ferrosilicate perovskite, $Mg_{1-y}Fe_ySiO_3$, and ferropericlase, $Mg_{1-x}Fe_xO$ (hereafter, Pv and Fp, respectively). In contrast, evidence based on solar and chondritic abundances suggests a deep lower mantle chemical transition into a pure Pv composition at ≈1,000 km depth (6). A chemical transition with wide topography, gentle, and diffuse changes in elasticity and density is also supported by geodynamic modeling (7). The discovery of the spin cross-over in Fp and Pv at lower mantle pressures (8, 9) introduces a new dramatic ingredient that demands a careful reexamination of these phases' elastic properties at appropriate conditions, the consequences for mantle elasticity, and reanalysis of lower mantle properties. This may, after all, support lower mantle models containing a chemical transition. Here, we show the effect of the spin cross-over on the bulk modulus and bulk velocity of Fp at high temperatures. We also show the effect it should have on the bulk modulus of a homogeneous lower mantle with pyrolite composition and confirm and justify the origin of anomalies in the elasticity of Fp recently demonstrated at room temperature (10). We point out that such an elastic anomaly might alter the activation energy for diffusion creep (11, 12) in Fp, which might affect mantle viscosity.

Results and Discussions

The high-spin (HS) to low-spin (LS) cross-over (13) in ferrous iron in Fp has been detected by several techniques at room temperature (8, 10, 14–18) and recently up to 2,000 K (19). For typical mantle compositions the cross-over may start as low as ≈35 GPa (18) and end as high as 75 GPa (8) at room temperature. The observed variations in the pressure range of the transition seem to be related to the variable degree of hydrostaticity in experiments. This pressure range broadens substantially with increasing temperature (19). This is actually a cross-over that occurs continuously (20, 21) passing through a mixed-spin (MS) state. Here, we extend the earlier thermodynamics formalism developed to investigate the spin cross-over in Fp (21) by including the spin-state-dependent vibrational properties. Equations of state do not have predictive quality unless they include vibrational effects. This is a particularly challenging task given the strongly correlated nature of this solid solution. We then obtain the high temperature compressibility and bulk velocity of Fp. We also address the potential effect the anomalous compressibility across the spin transition might have on the creep viscosity of Fp.

High-Temperature Properties. Inclusion of the vibrational contribution to the free energy improves considerably agreement between the experimentally measured (18, 19) and our predicted pressure and temperature-dependent spin populations and compression curves at room temperature (see supporting information (SI) Figs. S1 and S2). A description of the calculation and a more detailed analysis of these results are given in *SI Text* (Figs. S1–S5 and Tables S1–S5). The quality of our predictions can also be tested by inspecting the thermal expansivity, α, shown in Fig. 1. At low or very high pressures α has normal behavior because the system remains, respectively, in pure HS or LS states. The normal thermal expansivity of the HS state is essentially the same as that of MgO (22, 23) as observed experimentally (25). Within the range of validity of the quasiharmonic approximation (QHA) (1, 24), the magnitude of α at 0 GPa agrees very well with measurements for other concentrations (22). Throughout the spin cross-over α behaves anomalously. This type of anomaly has been measured in $LaCoO_3$ perovskite, another system that undergoes 2 spin cross-overs with increasing temperature at 0 GPa (26). The amplitude of the anomaly may be overestimated in our case because of the possibly narrower calculated cross-over range. As discussed in the *SI Text*, the uniform distribution of iron in our calculations underestimates iron–iron interaction, decreases the pressure range of the cross-over (18, 60), and increases the magnitude of the anomaly. Nevertheless, this effect is noticeable, could have significant consequences for the mantle geotherm, mantle dynamics, and temperature-induced lateral heterogeneities. Ultimately a full geodynamic simulation with self-consistent mineral physics parameters obtained on-the-fly will probably be necessary to answer these questions. Anomalies on several other thermodynamics quantities will be reported elsewhere (62).

The adiabatic bulk modulus, K_S, density, ρ, and bulk velocity, V_Φ, along several isotherms are shown in Fig. 2. Below 35 GPa, our calculated K_S and ρ are in excellent agreement with the

GEOPHYSICS

Fig. 1. Thermal expansivity of Fp along several isobars. Full (dashed) lines correspond to results within (outside) the (P and T) regime of validity of the QHA (1, 24). Circles and crosses are experimental values at 0 GPa for $Mg_{1-x}Fe_xO$ with $x = 0.0$ (22) and $x = 0.36$ (23), respectively.

adiabatic bulk modulus, K_S, and ρ measured at 300 K in the HS state for $X_{Fe} = 0.17$ (15). Inclusion of vibrational effects improves considerably the agreement with experiments. The remaining difference is consistent with the difference in iron concentration. There is a considerable reduction in K_S and V_Φ throughout the spin cross-over that is consistent with the reduction in bulk modulus of Fp with $X_{Fe} = 0.06$ (10) shown in the same figure. The difference in the magnitude of the anomaly is also consistent with the difference in iron concentration, i.e., approximately a factor of 3. The magnitude of the anomaly is

Fig. 2. Pressure dependence of the calculated adiabatic bulk modulus (*A*), K_S, and bulk wave velocity (*B*), V_ϕ and density, ρ, of $Mg_{1-x}Fe_xO$ ($x = 0.1875$) along several isotherms. Full (dashed) lines correspond to results within (outside) the (P and T) regime of validity of the QHA (1, 24). Experimental data for K_S on a sample with $X_{Fe} = 0.06$ (10) is shown in *A*. The calculated anomaly is approximately 3 times larger than the observed one. Crosses on *B* are experimental data at 300 K on a sample with $X_{Fe} = 0.17$ (15).

Fig. 3. Properties of $Mg_{1-x}Fe_xO$ ($x = 0.1875$) along a lower mantle geotherm (29). (*A*) Adiabatic bulk modulus, K_S; (*B*) bulk velocity, V_ϕ, and density, ρ; and (*C*) bulk modulus of an aggregate with pyrolite composition, K_{pyr}, compared with PREM's (30) bulk modulus, K_{PREM}. In *A* and *B*, full, dashed, and dotted lines correspond to properties computed in the MS, HS, and LS states, respectively. Shaded regions represent the uncertainties caused mainly by the uncertainty in the computed enthalpies of HS and LS states (see *SI Text*) and spin cross-over pressure at $T = 0$ K.

more noticeable at low temperatures: at 300 K the cross-over pressure range is $\approx 36-48$ GPa compared with the experimental one, $\approx 35-50$ GPa (17), or $\approx 50-75$ GPa (8, 10, 15–17, 19). Therefore, the difference between predictions and measurements are comparable to differences between experiments, but our results agree particularly well with the data of Fei et al. (18) (see Fig. S2).

Potential Effect of the Spin Cross-over Transition in Fp on the Mantle Bulk Modulus. The effect of the spin cross-over in Fp along a typical geotherm (28) is shown in Fig. 3 *A* and *B*. The anomalies in K_S (25 ± 6%) and V_ϕ (15 ± 7%) predicted by a purely elastic model start at ≈ 40 GPa ($\approx 1,000$ km depth) and are most pronounced $\approx 70 \pm 20$ GPa (1,600 ± 400 km), but the cross-over continues down to the core-mantle boundary (CMB) pressure with a possible reentrance into the HS state because of the

thermal boundary layer above the CMB (29). However, one should have in mind that anelastic effects might be enhanced in the region where the bulk modulus softens. In contrast, density increases smoothly throughout the entire pressure range of the lower mantle. The shaded areas correspond to possible values of these quantities due to uncertainties in the calculated static transition pressure and the narrower range of our transition pressure.

The net effect of the spin transition in Fp on the bulk modulus of a uniform aggregate with pyrolite composition (31) along a mantle geotherm (29) is shown of Fig. 3C. This comparison is made to elucidate and highlight an effect that may be quite subtle. We have adopted the first principles bulk modulus of Pv reported earlier by our group (1). The effect of iron on the bulk modulus of Pv without the effect of its own spin cross-over was included as reported in ref. 32, $K(x) = K_0(1 + bX_{Fe})$, where b varies linearly between 0.079 and 0.044 from 0 GPa to 136 GPa, respectively. Experimentally, Pv's bulk modulus is not noticeably affected by the spin cross-over (33). Theory predicts that LS ferrous iron will be displaced from the equilibrium HS site, and that the volume change will be quite insignificant throughout the cross-over (34). At 0 GPa the aggregate consists of 80 wt % of $Mg_{(1-x)}Fe_xSiO_3$, with $x = 0.12$, and 20 wt % of $Mg_{(1-y)}Fe_yO$, with $y = 0.1875$. This translates into a monotonic increase in vol % of Pv in the lower mantle, from 79.6 vol % to 80.8 vol % from 23 GPa to 120 GPa. The bulk modulus of the aggregate was computed by using the Voigt–Reuss–Hill average (35). Compared with PREM's bulk modulus (K_{PREM}) (30), K_{pyr} shows a subtle undulation, i.e., a reduction of $\approx 4 \pm 4\%$, which appears to be smoothed or cut through by PREM. The uncertainty in K_{pyr} is quite large and permits the signature of the spin cross-over in Fp to fall within the uncertainty of global seismic constraints (27). The effect of the spin cross-overs in Pv still needs to be better understood and more sensitive strategies need to be devised to identify the signature of this cross-over in Fp, which is a subtle one at lower mantle conditions. Nevertheless, given that (i) our predictions should offer an upper bound value for these anomalies, (ii) that this is a purely elastic model (see next section), and (iii) the overall accuracy of the calculation, K_{PREM} does not appear to be inconsistent with K_S of a uniform pyrolite aggregate with a spin cross-over in Fp along a typical adiabatic geotherm. The softening of the bulk modulus may be more noticeable in colder environments (slabs) and even less noticeable in hotter regions (superplumes).

Correlation Between Mantle Viscosity Structure and the Spin Cross-Over in Fp. The softening of K_S in Fp might also have an impact on mantle viscosity. Combination of a thermal convection model by using Newtonian viscous flow and seismic tomography data have implied the existence of a local minimum in mantle viscosity centered at $\approx 1,500$ km (36, 37). We notice the proximity of the viscosity minimum and of the predicted anomaly in the bulk modulus of Fp in the mantle (Fig. 3A). As a relatively minor, weaker phase comprising ≤ 20 vol % of Earth's lower mantle, the influence of Fp on viscosity depends critically on its distribution. In a poorly mixed system, Fp grains will be isolated from one another by Pv grains, which have a viscosity $\approx 10^3$ times that of Fp far from the spin cross-over (25). With Pv forming a load-bearing framework, the effect of Fp on viscosity will be modest. However, if phase separation occurs during large-strain deformation, Fp will markedly impact lower mantle viscosity. Recent shear deformation experiments on partially molten rocks, as well as on 2-phase rocks in which the viscosities of the 2 phases are significantly different, demonstrate a profound segregation of the constituent phases (28, 38). Mineralogical segregation and compositional layering are also observed in highly strained, naturally deformed rocks (39, 61). Bands rich in Fp, separated by regions rich in Pv, are thus anticipated in a deforming lower mantle. Once phase separation occurs, strain localizes in the weak, Fp-rich layers causing a significant decrease in viscosity relative to the viscosity of a homogenously mixed, 2-phase rock (41).

Here, we invoke an elastic strain energy model (ESEM) (11) for viscosity to estimate the potential impact of the bulk modulus softening on Fp's viscosity, η_{Fp}. A Newtonian subsolidus flow is assumed consistent with a diffusion creep deformation mode expected in the mantle and with the model used to infer lower mantle viscosity on the basis of convection-related and postglacial rebound data (36, 37). Fp's viscosity, η_{Fp}, is then:

$$\eta_{Fp} = A \, \exp\left(\frac{G^*}{k_B T}\right) \qquad [1]$$

where G^* is the extrinsic activation energy for the dominant deformation mechanism, i.e., ionic diffusion, and A is a constant. At a depth z, $\eta_{Fp}(z)$, should be (12):

$$\eta_{Fp}(z) = \eta_{Fp}(z_0)\exp\left(\frac{G^*(z)}{k_B T(z)} - \frac{G^*(z_0)}{k_B T(z_0)}\right) \qquad [2]$$

where $\eta_{Fp}(z_0)$ and $G^*(z_0)$ are Fp's viscosity and activation energy at a reference depth z_0, here assumed to be the top of the lower mantle.

The ESEM relates the activation energy for diffusion, $G^*(z_0)$, with the shear and bulk modulus of the system. The ionic diffusion process induces bond stretching and/or shearing depending on the diffusion path. As such, the diffusion barrier is related to different extents to shear and bulk modulus. This is usually described as a parameterized dependence on the pure shear and dilatational contributions, $G_s^*(z)$ and $G_D^*(z)$, to the activation energy,

$$G^*(z) = \delta G_s^*(z) + (1 - \delta)G_D^*(z) \qquad [3]$$

where δ is a free parameter. The other quantities are (12):

$$\frac{G_s^*(z)}{G_s^*(z_0)} = \frac{V(z)\mu(z)}{V(z_0)\mu(z_0)} \quad \text{and} \quad \frac{G_D^*(z)}{G_D^*(z_0)} = \frac{V(z)K(z)}{V(z_0)K(z_0)} \qquad [4]$$

with $\mu(z)$, $K(z)$, and $V(z)$ being shear and bulk moduli and volume, respectively. This model works well for metals, but the relationship between the diffusion barrier and the elastic moduli for ionic systems may not be this simple, even though there are indications that this model describes well the high-pressure and high-temperature behavior of diffusion in MgO (42). Nevertheless, this model expresses a relationship that is very likely to exist in some similar form between viscosity and elastic moduli. Despite consistency between experimental data (42) and first principles results of migration barriers in MgO (43–45), similar investigations in Fp are still necessary to clarify this point. Much less is known about the shear modulus at this point. Room temperature measurements (10) have indicated that the shear modulus also softens throughout the spin cross-over, but this has not been confirmed by theory or by more recent Brillouin scattering data (46). Therefore, the situation remains controversial and shear deformation may enhance or damp the bulk modulus related viscosity anomaly. Experimental data (42) and modeling (43–45) have suggested that $G^*(z_0) \approx 300$–330 kJ/mol at uppermost lower mantle conditions ($z_0 = 660$ km, $P = 23$ GPa, $T = 2,000$ K). We then assume $G^*(z_0) = 315$ kJ/mol (42). Even if the shear modulus were known with certainty at this point, one would still have to estimate δ to infer the impact of the shear modulus on Fp's viscosity.

The impact of the bulk modulus softening on Fp's viscosity predicted by a purely dilatational ESEM ($\delta = 0$ in Eq. **11**) is shown in Fig. 4 compared with the relative changes in lower
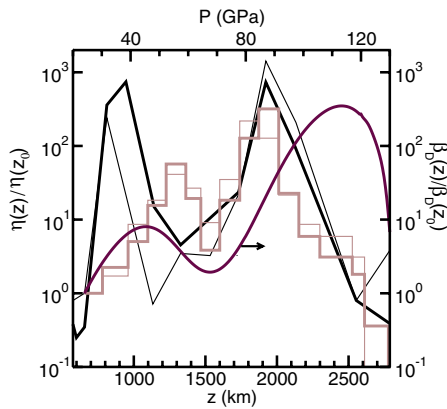
$$\frac{V(n)}{K(n)} = n\frac{V_{\text{LS}}}{K_{\text{LS}}} + (1-n)\frac{V_{\text{HS}}}{K_{\text{HS}}} - (V_{\text{LS}} - V_{\text{HS}})\left.\frac{\partial n}{\partial P}\right|_T \quad [6]$$

where $n = n(P,T)$ is the LS fraction, and V_{LS}, V_{HS}, K_{LS}, and K_{HS} are the equilibrium volume and isothermal compressibility of pure LS and HS states. Eq. **6** differs from the weighted average of the compressibilities by an additional term caused by the pressure dependence of $n(P,T)$. This last term is ultimately responsible for the bulk modulus anomaly reported recently (10). According to Eqs. **5** and **6**, the properties of Fp in the MS state may be determined from those of the LS and HS states plus the LS fraction, $n(P,T)$, all of which must be computed by first principles.

In contrast to the previous thermodynamics treatment (21) we now include vibrational effects. It is impossible to address thermodynamics properties without them. The other approximations used in ref. 21 to compute $n(P,T)$ are retained. They are:

1. The magnetic entropies are $S_{\text{HS}}^{\text{mag}}(n) = k_B X_{\text{Fe}} \ln[m(2S+1)]$ and $S_{\text{LS}}^{\text{mag}} = 0$ for the HS and LS states, respectively. S and m are, respectively, the total spin quantum number and orbital degeneracies of the HS ($S = 2$ and $m = 3$) and LS ($S = 0$ and $m = 1$) states.
2. The HS-LS configuration entropy is $S_{\text{conf}} = -k_B X_{\text{Fe}} [n \ln n + (1-n)\ln(1-n)]$. Fluctuations in $n(P,T)$ are insignificant given the finite sample sizes. Because configurations are not expected to be static in this solid solution, this formula implicitly assumes the ergodic hypothesis, i.e., time and ensemble averages are equal.
3. The Mg/Fe configuration entropy is insensitive to spin state.

$n(P,T)$ is then obtained by minimizing the Gibbs free energy with respect to n. This leads to:

$$n(P, T) = \frac{1}{1 + m(2S+1)\exp\left[\dfrac{\Delta G_{\text{LS}-\text{HS}}^{\text{stat}+\text{vib}}}{X_{\text{Fe}} K_B T}\right]} \quad [7]$$

where $\Delta G_{\text{LS}-\text{HS}}^{\text{stat}+\text{vib}}(P, T)$ is the difference between the static plus vibrational contributions to the free energy of the LS and HS states, X_{Fe} is the concentration of iron (here, 0.1875). Therefore, to obtain $\Delta G_{\text{LS}-\text{HS}}^{\text{stat}+\text{vib}}(P, T)$ and $n(P,T)$ it is necessary first to obtain the vibrational spectrum and free energies of pure spin states within the QHA.

Vibrational Virtual Crystal Model (VVCM). The thermal properties of Fp in pure spin states were computed by using the QHA (55) in which the Helmholtz free energy is given by:

$$F(V, T) = \left[U(V) + \sum_{qj} \frac{\hbar\omega_{qj}(V)}{2} \right]$$
$$+ k_B T \sum_{qj} \ln\left[1 - \exp\left(-\frac{\hbar\,\omega_{qj}(V)}{k_B T} \right) \right] \quad [8]$$

where $U(V)$ is the volume-dependent static total internal energy obtained by first principles and $\omega_{qj}(V)$ is the corresponding volume-dependent phonon spectrum.

Current methodological limitations preclude a direct computation of the vibrational density of states (VDOS) of Fp within the first principles LDA+U approach (56). To circumvent this problem we developed a VVCM. The VC concept involves the replacement the atomic species forming the solid solution, in this case, magnesium and HS or LS irons, by an "average cation" that can reproduce the properties of the solid solution. Here, we develop a VC to compute only vibrational and thermodynamics properties. We are not aware of previous similar attempts in the literature. The development of successful VVCMs would be extremely useful to bypass the difficult problem of computing VDOS for numerous configurations involving hundreds of atoms representative of solid solutions, especially strongly correlated ones, so common in minerals.

The VVCMs corresponding to the pure HS and LS states consist of 2 atoms per cell in the rocksalt structure: oxygen and a virtual (cation) atomic species with a mass

$$M_{\text{VC}}^{\text{cation}} = (1 - X_{\text{Fe}})M_{\text{Mg}} + X_{\text{Fe}}M_{\text{Fe}} \quad [9]$$

Fig. 4. Viscosity of ferropericlase along a mantle geotherm (29) compared with mantle viscosity models (36, 37). Thin and thick black lines (37) were derived from convection related data extracted from geoid inversion and 2 distinct tomography models, refs. 47 and 48, respectively. Thin and thick light-brown lines (37) included also glacial rebound data in the derivation of the viscosity models. The tomography models were the same as those used in ref. 37. Thick maroon line is the relevant property of Fp computed in the MS state. $\beta_D(z)$ is the contribution of the dilatational component of the activation energy, $G_D(z)$, to $\eta_{\text{Fp}}(z)$ ($\delta = 0$ only).

mantle viscosity, $\eta(z)$ (36, 37), with depth. All profiles have accentuated minima at $\approx$1,400–1,600 km. The decrease in Fp's viscosity near the CMB in our model is caused by the reentrance into the HS state owing to the thermal boundary layer (29) above the CMB, whereas the more drastic reduction in mantle viscosity beyond 2,000 km may be related with numerous additional factors (40), such as the approaching postperovskite transition or the temperature profile. It appears to depend also on the inversion model used to obtain the viscosity (36, 37).

The bulk modulus anomaly in Fp may not only affect the viscosity and dynamics of the mantle (49) but also its overall state (50) and properties. In general, it is anticipated that properties of Fp related with ionic diffusion, such as ionic conductivity, should improve in the MS state owing to its enhanced compressibility (anomalously "soft" bonds), even though ionic conductivity is not the prevailing electrical conduction mechanism at conditions explored so far (51–53). In contrast, such properties should deteriorate in the LS state compared with the HS state because of the reduction in lattice parameter. Heat (lattice) conductivity, instead, is expected to follow the opposite trend: it should be boosted in the LS state and damped in the MS state in comparison with the HS state. Seismic attenuation also results from an activated diffusion process. Experimentally, the attenuation Q-factor is related to viscosity as $Q \propto \eta^\beta$, where $0.2 < \beta < 0.9$ (54). Given this relation and the possibility of viscosity reduction by a factor of $\approx$10–50 in the middle of the cross-over, one would normally expect Q^{-1} in Fp to increase by a factor of $\approx$10–30 in the same regime. However, it is unclear whether this relationship between Q-factor and viscosity holds for materials undergoing spin cross-over, but in principle one should also expect enhanced attenuation throughout the cross-over. Several aspects of the spin cross-over in Fp still need to be investigated before its consequences are better understood.

Methods

Thermodynamics of the Cross-Over Transition. We treat Fp in the MS state as an ideal solid solution of HS and LS states. This approximation seems to be well justified by the concentration-independent static spin transition pressure for concentrations up to $x = 0.1875$ (21). Therefore:

$$V(n) = nV_{\text{LS}}(P, T) + (1-n)V_{\text{HS}}(P, T) \quad [5]$$

where M_{Mg} and M_{Fe} are, respectively, the atomic masses of magnesium and iron, with the latter being independent of the iron's spin state. The interactions of the VC cation in the solid are modeled for the purpose of computing vibrational and thermodynamics properties only.

The VVCMs are essentially periclase, MgO with modified interatomic force constants that reproduce the elastic constants of HS or LS Fp and cation masses as in Eq. **9**. The force constants of periclase were previously computed by first principles and produce excellent phonon dispersions (57, 58). The force constants of the HS or LS VCs are obtained by matching the elastic constants extracted from the acoustic phonon dispersions (57, 58)[†] close to $k = 0$ to the elastic constants of HS and LS calculated by first principles. There is a linear relationship between force constants $D_{\mu\nu}(R^{ij})$ and elastic constants $C_{\sigma\tau\alpha\beta}$ (59):

$$C_{\sigma\tau\alpha\beta}(V) = \sum_{(i,j),(\mu,\nu)} a^{ij}_{\mu\nu,\sigma\tau\alpha\beta}(V)D^{ij}_{\mu\nu}(V). \qquad [10]$$

Here, Greek letters refer to Cartesian indices, $C_{\sigma\tau\alpha\beta}(V)$ are the volume-dependent elastic constants in cartesian notation, while $D^{ij}_{\mu\nu}$ are the interatomic force constants between atoms i and j separated by R^{ij} when displaced in directions μ and ν, respectively. The sum in Eq. **10** is over all atomic pairs (i,j) and $a^{ij}_{\mu\nu,\sigma\tau\alpha\beta}(V)$ are a set of volume-dependent constants. Because of symmetry constrains, many of the $a^{ij}_{\mu\nu,\sigma\tau\alpha\beta}$ constants vanish. Eq. **10** is a convergent summation since the force constants vanish rapidly with the interatomic distances. The convergence in Eq. **10** is guaranteed if the force constants vanish faster than $1/R^5$, where R is the interatomic separation (59).

The force constants defined as

$$D^{ij}_{\mu\nu} = \frac{\partial^2 E(R^{ij})}{\partial R^{\mu}_i \partial R^{\nu}_j} \qquad [11]$$

are used to compute the phonon spectrum at each volume:

[†]The static elastic constants of Fp in pure spin states were computed by first principles by using the usual stress versus strain relations. The lower symmetry of the solid solution is restored by resymmetrization of the elastic constant tensor as described in ref. 32.

$$\det\left|\frac{D^{ij}_{\mu\nu}(V)}{\sqrt{M_i M_j}} - \omega^2\right| = 0 \qquad [12]$$

and we need to obtain $D^{ij}_{\mu\nu}(V)$ for HS and LS VVCMs. Fp and periclase have only 3 elastic constants, C_{11}, C_{12}, and C_{44} (Voigt notation) (35). We may modify 3 force constants of periclase independently to reproduce the static elastic constants of HS and LS Fp. We modified the 3 largest interatomic force constants of periclase, D^{11}_{xx} (Mg–O nearest neighbor longitudinal interaction), D^{11}_{xy} (Mg–Mg nearest magnesium interaction), and D^{12}_{xy} (the Mg–O nearest neighbor transverse interaction). All other force constants of MgO are at least 1–2 orders of magnitude smaller and remained unchanged. Changes in those force constants have only a minor effect on the elastic constants. More details of the VVCM developed here will be discussed elsewhere (62).

A comparison between the static bulk modulus obtained by fitting an equation of state to the energy versus volume relation in HS and LS $Mg_{1-x}Fe_xO$ ($x = 0.1875$) and the bulk modulus obtained from the elastic constants of the respective VCs is shown in Fig. S3. The virtual crystals produce distinct vibrational density of states (VDOS) for periclase, HS, and LS Fp (see Fig. S4). The acoustic mode dispersions of the HS and LS VVCMs are precisely the same as those of HS and LS Fp. This ensures that thermodynamics calculations are carried out with the correct VDOS at low frequencies, which matter the most, and with a reasonably good weight-averaged VDOS at high frequencies as well. The VVCM should offer more accurate thermodynamics properties than a Debye-like model because of the more detailed structure of the VDOS. We considered carefully the pressure/temperature range of validity of the QHA. Full and dashed lines in all figures correspond to conditions within and outside its range of validity, respectively. The upper temperature limit of the QHA is adopted as the lowest temperature of the inflection points in the thermal expansivity of pure LS and HS Fp at every pressure (1, 24), i.e., $\partial^2\alpha/\partial T^2|_P = 0$.

1. Wentzcovitch RM, et al. (2004) Thermoelastic properties of MgSiO₃-perovskite: Insights on the nature of the Earth's lower mantle. *Phys Rev Lett* 92:018501–018504.
2. E. Mattern, et al. (2005) Lower mantle composition and temperature from mineral physics and thermodynamic modeling. *Geophys J Int* 160:973–990.
3. Matas J, et al. (2007) (2007) On the bulk composition of the lower mantle: Predictions and limitations from generalized inversion of radial seismic profiles. *Geophys J Int* 170:764–780.
4. Wentzcovitch RM, Tsuchiya T, Tshuchiya J (2006) MgSiO₃ postperovskite at D″conditions. *Proc Natl Acad Sci USA* 103:543–546.
5. Wookie J, et al. (2005) Efficacy of the post-perovskite phase as an explanation for lowermost-mantle seismic anomalies. *Nature* 438:1004–1007.
6. Williams Q, Knittle E (2005) The uncertain major element bulk composition of earth's mantle. *AGU Geophysical Monograph 160*, ed van der Hilst RD, Bass JD, Matas J, Trampert J (American Geophysical Union, Washington, DC), pp 187–199.
7. Kellogg LH, Hager BH, van der Hilst RD (1999) Compositional stratification in the deep mantle. *Science* 283:1881–1884.
8. Badro J, et al. (2003) Iron partitioning in Earth's mantle: Toward a deep lower mantle discontinuity. *Science* 300:789–791.
9. Badro J, et al. (2004) Electronic transitions in perovskite: Possible Nonconvecting layers in the lower mantle. *Science* 305:383–386.
10. Crowhurst JC, et al. (2008) Elasticity of (Mg,Fe)O through the spin transition of iron in the lower mantle. *Science* 319:451.
11. Sammis CG, Smith JC, Schubert G (1981) A critical assessment of estimation methods for activation volume. *J Geophys Res* 86:10707–10718.
12. Ellsworth K, Schubert G, Sammis CG (1985) Viscosity profile of the lower mantle. *Geophys J R Astr Soc* 83:199–213.
13. Gutlich P, Goodwin HA (2004) *Spin Crossover Transitions*, Topics in Current Chemistry (Springer, Berlin), Vol 233.
14. Kantor IY, Dubrovinsky LS, McCammon CA (2006) Spin crossover in (Mg,Fe)O: A Mössbauer effect study with an alternative interpretation of X-ray emission spectroscopy data. *Phys Rev B* 73:100101–100104.
15. Lin JF, et al. (2005) Spin transition of iron in magnesiowüstite in the Earth's lower mantle. *Nature* 436:377–380.
16. Speziale S, et al. (2005) Iron spin transition in Earth's mantle. *Proc Natl Acad Sci USA* 102:17918–17922.
17. Lin JF, et al. (2006) Sound velocities of ferropericlase in the Earth's lower mantle. *Geophys Res Lett* 33:L22304.1–L22304.5.
18. Fei Y, et al. (2007) Spin transitions and equations of state of (Mg,Fe)O solid solutions. *Geophys Res Lett*, 1029/2007GL030712.
19. Lin JF, et al. (2007) Spin transition zone in the Earth's lower mantle. *Science* 317:1740–1743.
20. Sturhahn W, Jackson JM, Lin JF (2005) The spin state of iron in minerals of Earth's lower mantle. *Geophys Res Lett* 32: L12307.1–L12307.5.
21. Tsuchiya T, et al. (2006) Spin transition in magnesiowüstite in Earth's lower mantle. *Phys Rev Lett* 96:198501.
22. Touloukian YS, et al. (1977) *Thermophysical Properties of Matter* (Plenum, New York), Vol 13.
23. van Westrenen W, et al. (2005) Thermoelastic properties of (Mg₀.₆₄Fe₀.₃₆)O ferropericlase based on in situ X-ray diffraction to 26.7 GPa and 2173 K. *Phys Earth Planet Interiors* 151:163–176.
24. Carrier P, Wentzcovitch RM, Tsuchiya J (2007) First-principles prediction of crystal structures at high temps using the quasiharmonic approximation. *Phys Rev B* 76:064116.1–064116.5.
25. Yamazaki D, Karato S-i (2001) Some mineral physics constraints on the rheology and geothermal structure of Earth's lower mantle. *Am Mineral* 86:381–391.
26. Radaelli PG, Cheong S-W (2002) Structural phenomena associated with the high spin transition in LaCoO₃. *Phys Rev B* 66:094408-1–094408-9.
27. Masters G (2008) On the possible (1D) seismological signature of the spin crossover in ferropericlase. *EOS Trans AGU* 89(Fall Meet Suppl):MR23A-04 (abstr).
28. Barnhoorn A, et al. (2005) Strain localization in bimineralic rocks: Experimental deformation of synthetic calcite-anhydrite aggregates. *Earth Planet Sci Lett* 240:748–763.
29. Boehler R (2000) High-pressure experiments and the phase diagram of lower mantle and core materials. *Rev Geophys* 38:221–245.
30. Dziewonski AM, Anderson DL (1981) Preliminary reference Earth model (PREM). *Phys Earth Planet Interiors* 25:297–356.
31. McDonough WF, Sun S-s (1995) The composition of the Earth. *Chem Geol* 120:223–253.
32. Kiefer B, Stixrude L, Wentzcovitch RM (2002) Elasticity of (Mg,Fe)SiO₃-perovskite at high pressures. *Geophys Res Lett* 29:1539.
33. Lundin S, et al. (2008), Effect of Fe on the equation of state of mantle silicate perovskite over 1 Mbar. *Phys Earth Planet Interiors* 168:97–102.
34. Umemoto K, Wentzcovitch RM (2008) Spin transition in (Mg,Fe)SiO₃ perovskite under pressure, *Earth Planet Sci Lett* 276:198–206.
35. Hill R (1952) The elastic behavior of a crystalline aggregate. *Proc Phys Soc London Ser A* 65:349–354.

GEOPHYSICS

36. Forte AM, Mitrovica JK (2001) Deep-mantle high-viscosity flow and thermochemical structure inferred from seismic and geodynamic data. *Nature* 410:1049–1056.
37. Mitrovica JK, Forte AM (2004) A new inference of mantle viscosity based upon joint inversion of concection and glacial isostatic adjustment data, *Earth Planet Sci Lett* 225:177–189.
38. Holtzman BK, et al. (2003) Melt segregation and strain partitioning: Implications for seismic anisotropy and mantle flow. *Science* 301:1227–1230.
39. Williams ML, et al. (2000) Microstructural tectonometamorphic processes and the development of gneissic layering: A mechanism for metamorphic segregation. *J Metamorph Geol* 18:41–57.
40. Sammis CG, et al. (1977) Viscosity-depth profile of the earth's mantle: Effects of polymorphic phase transitions. *J Geophys Res* 82:3747–3761.
41. Holtzman BK, Kohlstedt DL, Morgan JP (2005) Viscous energy dissipation and strain partitioning in partially molten rocks. *J Petrol* 46:2569–2592.
42. Van Orman JA, et al. (2002) Diffusion in MgO at high pressures: Constraints on deformation mechanisms and chemical transport at the core-mantle boundary. *Geophys Res Lett*, 10.1029/2002GL016343.
43. Ita J, Cohen R (1997) Effects of pressure on diffusion and vacancy formation in MgO from non-empirical free energy integrations. *Phys Rev Lett* 79:3198–3201.
44. Karki B, Khanduja G (2006) Vacancy defects in MgO at high pressure. *Am Miner* 91:511–516.
45. Ito Y, Toriumi M (2007) Pressure effect of self-diffusion in periclase (MgO) by molecular dynamics. *J Geophys Res*, 10.1029/2005JB003685.
46. Wang J, Sanchez-Valle C, Bass J (2008) Single crystal elasticity of Al-bearing frropericlase at high pressures up to 81 GPa. *EOS Trans AGU* 89(Fall Meet Suppl):MR31A-1834 (abstr).
47. Grand SP, van der Hilst RD, Widyantoro S (1997) Global seismic tomography: A snapshot of convection in the earth. *Geol Soc Am Today* 7:1.
48. Ekstrom G, Dziewonski AM (1998) The unique anisotropy of the Pacific upper mantle. *Nature* 394:168–172.
49. Yuen DA, et al. (1996) *Seismic Modeling of the Earth's Structure*, ed Boschi E, Ekstrom G, Morelli A (Editrice Compositori, Bologna, Italy), pp 463–506.
50. Cammarano F, et al. (2005) Is a pyrolitic adiabatic mantle compatible with seismic data? *Earth Planet Sci Lett* 232:227–243.
51. Dobson DP, Brodholt JP (2000) The electrical conductivity of the lower mantle phase magnesiowüstite at high temperatures and pressures. *J Geophys Res* 105:531–538.
52. Lin J-F, et al. (2007) Electrical conductivity of the lower mantle ferropericlase across the electronic spin transition, *Geophys Res Lett*, 10.1029/2007GL030523.
53. Ohta K, et al. (2007), The effect of iron spin transition on electrical conductivity at (Mg,Fe)O magnesiowüstite. *Proc Jpn Acad Ser B* 83:97–100.
54. Karato S-I (2003) *The Dynamic Structure of the Deep Earth*: *An Interdisciplinary Approach* (Princeton Univ Press, Princeton, NJ).
55. Wallace D (1972) *Thermodynamics of Crystals* (Wiley, New York).
56. Cococcioni M, de Gironcoli S (2005) Linear response approach to the calculation of the effective interaction parameters in the LDA+U method. *Phys Rev B* 71:035105.
57. Karki BB, Wentzcovitch RM., de Gironcoli S, Baroni S (2000) High-pressure lattice dynamics and thermoelasticity of MgO. *Phys Rev B* 61:8793–8800.
58. Karki BB, Wentzcovitch RM, de Gironcoli S, Baroni S (1999) First principles determination of elastic anisotropy and wave velocities of MgO at lower mantle conditions. *Science* 286:1705.
59. Ashcroft NW, Mermin ND (1976) *Solid State Physics* (Holt, Rinehart and Winston, New York).
60. Persson K, Bengtson A, Ceder G, Morgan D (2006) Ab initio study of the composition dependence of the pressure-induced spin transition in the $(Mg_{1-x},Fe_x)O$ system. *Geophys Res Lett* 33:L16306.
61. Larkin LM, Zimmerman ME, Kohlstedt DL (2005) Phase separation during deformation of a two-phase rock, *EOS Trans AGU* 86(Fall Meet Suppl):T41C-1320 (Abstr).
62. Wu Z, et al. (2008) Thermodynamics properties of ferropericlase, *Phys Rev B*, in press.